Materials Science & Engineering A 766 (2019) 138350

Contents lists available at ScienceDirect

Materials Science & Engineering A

journal homepage: www.elsevier.com/locate/msea

Effect of spark plasma sintering and high-pressure torsion on the microstructural and mechanical properties of a Cu–SiC composite

P. Bazarnik[a,*], S. Nosewicz[b], B. Romelczyk-Baishya[a], M. Chmielewski[c], A. Strojny Nędza[c], J. Maj[b], Y. Huang[d,e], M. Lewandowska[a], T.G. Langdon[e]

[a] Warsaw University of Technology, 141 Woloska Str., 02-507, Warsaw, Poland
[b] Institute of Fundamental Technological Research, Polish Academy of Sciences, 5B Pawinskiego, 02-106, Warsaw, Poland
[c] Institute of Electronic Materials Technology, 133 Wolczynska Str, 01-919, Warsaw, Poland
[d] Department of Design and Engineering, Faculty of Science and Technology, Bournemouth University, Poole, Dorset, BH12 5BB, UK
[e] Materials Research Group, Department of Mechanical Engineering, University of Southampton, Southampton, SO17 1BJ, UK

ARTICLE INFO

Keywords:
Copper
Silicon carbide
High-pressure torsion
Spark plasma sintering
Thermal conductivity

ABSTRACT

This investigation examines the problem of homogenization in metal matrix composites (MMCs) and the methods of increasing their strength using severe plastic deformation (SPD). In this research MMCs of pure copper and silicon carbide were synthesized by spark plasma sintering (SPS) and then further processed via high-pressure torsion (HPT). The microstructures in the sintered and in the deformed materials were investigated using Scanning Electron Microscopy (SEM) and Scanning Transmission Electron Microscopy (STEM). The mechanical properties were evaluated in microhardness tests and in tensile testing. The thermal conductivity of the composites was measured with the use of a laser pulse technique. Microstructural analysis revealed that HPT processing leads to an improved densification of the SPS-produced composites with significant grain refinement in the copper matrix and with fragmentation of the SiC particles and their homogeneous distribution in the copper matrix. The HPT processing of Cu and the Cu–SiC samples enhanced their mechanical properties at the expense of limiting their plasticity. Processing by HPT also had a major influence on the thermal conductivity of materials. It is demonstrated that the deformed samples exhibit higher thermal conductivity than the initial coarse-grained samples.

1. Introduction

Metal matrix composites (MMCs) are lightweight structural materials which often exhibit unique properties such as enhanced strength and hardness [1,2], wear [3] and corrosion resistance [4–6] together with excellent electrical and thermal properties [6–8]. Various MMC systems have been studied and an enhancement of a range of material properties was reported thereby making these materials attractive for use in a wide range of applications including in the aerospace, automotive and electronics sectors [9,10].

Recently, significant interest has been directed towards the fabrication of copper-based composites [4,6–8,11–14]. Copper and its alloys exhibit excellent thermal and electrical conductive properties but, due to their poor mechanical properties of very low wear resistance and low yield strength, especially at elevated temperature, their use is restricted in many industrial applications. Therefore, Cu-based MMCs reinforced with ceramic particles are now under consideration as promising candidate materials for applications requiring high thermal conductivity and thermal stability together with excellent wear resistance. The incorporation of ceramic particulate reinforcements, such as SiC, may significantly improve the thermal and some of the mechanical properties as well as the wear resistance without any major deterioration in the thermal and electrical conductivities of the matrix [5,15,16]. The Cu–SiC MMCs appear to be promising engineering materials because they offer a combination of both the superior ductility and toughness of the copper matrix together with the high strength, high Young's modulus and exellent wear resistance of the SiC reinforcement. To date, Cu–SiC composites have been used extensively as welding electrodes, electrical contacts, and switches and in electronic packaging [17].

Several different techniques have been developed to synthesize MMCs where these methods include stir casting [18,19], spray forming [18,20], squeeze casting [18,21] and powder metallurgy [18,22]. In practice, powder metallurgy techniques such as hot isostatic pressing

* Corresponding author.
E-mail address: Piotr.Bazarnik@pw.edu.pl (P. Bazarnik).

https://doi.org/10.1016/j.msea.2019.138350
Received 21 July 2019; Received in revised form 26 August 2019; Accepted 27 August 2019
Available online 28 August 2019
0921-5093/

(HIP) [23], hot pressing (HP) [24] and spark plasma sintering (SPS) [18,25] are especially promising because of the attractive properties of the processed samples. In an earlier study, it was demonstrated that the microstructure and mechanical properties of Cu–SiC MMCs depend strongly on the nature of the sintering technique [15,26]. Specifically, the optimum densification, and therefore the best mechanical properties of Cu–SiC MMCs, was reported after SPS processing [15]. Nevertheless, MMCs obtained via powder metallurgy processing may have some disadvantages, including large microstructural inhomogeneities in the particle distributions, the presence of some residual porosity even after SPS processing [15] and in many cases a weak connection between the particles and the metal matrix. It is well established that structural inhomogeneity and residual porosity will significantly degrade the formability and ductility, thereby making these materials prone to premature failure.

In order to uniformly distribute the ceramic reinforcing particles within the metal matrix and to densify the sintered materials, it is feasible to use conventional deformation processes such as rolling or hot extrusion. However, in many cases the deformation level generated through these techniques is not sufficient to improve the microstructural homogeneity. For example, there is evidence that the improvement of homogeneity in MMCs requires strains higher than ~4 [27–29] which cannot be obtained in conventional rolling and hot extrusion processes.

Recently, severe plastic deformation (SPD) processes were used to fabricate MMCs and improve their homogeneity [30–45]. Moreover, SPD procedures increase the strength of the composites through a reduction in grain size in the matrix metal. A number of SPD methods were developed, such as high-pressure torsion (HPT) [46], equal-channel angular pressing (ECAP) [47], accumulative roll bonding (ARB) [48] and hydrostatic extrusion (HE) [49,50]. Among these methods, HPT is regarded as reasonably ideal for achieving good homogenization of the MMCs because of the ability to generate extremely high strains of typically more than 200 at 10 revolutions. This process has been widely used in the processing of nano- and micro-sized metals, metal alloys and their powders [51–57], intermetallics [58,59] and MMCs [30–32,38–45,60,61]. However, there are to date only a limited number of experimental studies on the HPT processing of Cu–SiC composites [62–64]. Moreover, there is a lack of information regarding the thermal conductivity of MMCs fabricated by SPD techniques.

Therefore, the purpose of this study was to investigate the fabrication of novel MMCs using HPT to provide homogenization of sintered Cu–SiC composites having different volume fractions of the SiC reinforcement. The strength, microhardness and thermal conductivity were examined and the effect of refinement of the matrix grains and the SiC particles on the thermal conductivity and mechanical properties was also evaluated.

2. Experimental

A regular-shaped copper powder (produced by NewMet Koch) with a purity of 99.99% and 40 μm average particle size was used as a matrix. The composites were reinforced by silicon carbide particles with a purity of 99.99% (Saint-Gobain, France) having average particle sizes of about 80 μm and theparticle size ranges from 30 μm to 130 μm.

The powders were mixed in a planetary mill (Pulverisette 6) using processing parameters of a rotational speed of 100 rpm, a time of mixing of 2 h and a ball-to-powder ratio (BPR) of 5:1. A milling medium was not used during the mixing. Two compositions of the powder mixtures were prepared with the following Cu to ceramic phase content (vol%): 90%Cu–10%SiC, 80%Cu–20%SiC.

The powders were consolidated by the SPS technique using a graphite die with a sample diameter of 10 mm and height of 10 mm. The sintering process was carried out at a temperature of 950 °C in an argon atmosphere with a heating rate of 100 °C/min and a 10 min holding time at maximum temperature at a pressure of 150 MPa. As a reference, a sample of pure copper was sintered under the same conditions.

The sintered samples were cut to discs with thicknesses of 1 mm and then subjected to HPT processing. This processing was conducted under an applied pressure of 6.0 GPa at room temperature under quasi-constrained conditions [65] where there is a small outflow of material around the periphery of the disc during the processing operation. Discs were torsionally strained by rotating the lower anvil at 1 rpm through 20 revolutions each.

The microstructures of the Cu and Cu–SiC composites were examined using scanning electron microscopy (SEM) (Hitachi SU-8000) operating at 10 kV. The images were taken in secondary electron (SE) and in back-scattered electron (BSE) modes. The SEM observations were performed on cross-sectional planes in the edge regions and also at ~0.5 mm from the disc edge. Detailed microstructural observations from selected areas were performed using a Cs-corrected dedicated high-resolution scanning transmission electron microscope (STEM) (Hitachi HD-2700). The STEM images were taken in bright-field (BF) and high-angle annular dark field (HAADF) modes. The samples for STEM observations were cut using the focussed ion beam (FIB) technique with a Hitachi NB5000 microscope. All microstructures were evaluated quantitatively using a computer-aided image analyser. The grain size was described by the equivalent grain diameter, d_{eq}, defined as the diameter of a circle with a surface area equal to the surface area of the grain.

To evaluate the changes in the mechanical properties after HPT processing, microhardness tests were performed on the polished surfaces of discs using an FM-300 microhardness tester equipped with a Vickers indenter. Measurements were taken under a load of 200 g and a dwell time of 10 s along randomly-selected diameters on each disc with a spacing of 0.3 mm between the measuring points. The results were plotted in the form of the hardness profiles. The study of mechanical properties was complemented by tensile testing conducted at room temperature using a Zwick 005 universal testing machine under displacement control at a strain rate of $1.0 \times 10^{-3}\,s^{-1}$. For proper strain estimation, Digital Image Correlation (DIC) was applied [66]. A CCD camera operating at 4fps with a Pentax lens was placed in front of the sample. The image acquisition by AVT software was synchronized with the beginning of each tensile test. Based on the load - displacement data, the yield stress (YS), ultimate stress (UTS) and the elongation to failure were determined.

The thermal conductivity of the processed composites was measured with the use of a laser pulse technique [67]. This was performed using an LFA 457 device by Netzsch over the temperature range of 50–300 °C in an argon atmosphere. The value of the thermal conductivity (TC) was calculated using the following equation:

$$\lambda = \rho \cdot c_p \cdot D \quad (1)$$

where λ is the thermal conductivity in W/mK, ρ is the density in g/cm^3, c_p is the specific heat in J/gK and D is the diffusivity in mm^2/s. The value of the specific heat was determined based on the rule of mixtures.

All of the results obtained for the samples after HPT processing were compared with data for the initial material after SPS processing.

3. Results

3.1. Microstructure evolution

Figs. 1–2 show representative images of the initial microstructures of pure Cu, Cu–10SiC and Cu–20SiC samples after SPS processing. The microstructure in the pure Cu sample after SPS is inhomogeneous and exhibits a bimodal character as illustrated in Fig. 1a with low magnification. The grain structure consists of two types of grains: (1) coarse grains having diameters of ~210 μm and occupying ~70% of the sample volume and (2) fine grains with an average grain size of

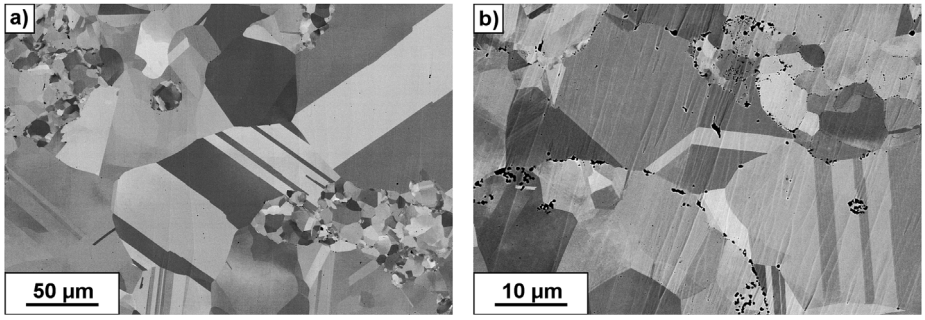

Fig. 1. SEM images of the microstructures of pure Cu after SPS processing at low (a) and high (b) magnifications.

~3.4 µm. Also, numerous twins are visible in the microstructure. Some residual porosity is visible in the copper matrix, as presented in Fig. 1b with high magnification where the black regions in the BSE image are pores. These pores have size ranges between ~0.5–2.0 µm and they are located mainly at the contact surfaces of the primary powder particles.

The structures of the Cu–10SiC and Cu–20SiC composites in Fig. 2 were more uniform. Microstructure observations show that the SiC reinforcement phase is fairly uniformly distributed throughout the sample volume with only a few clusters of SiC particles visible in the Cu matrix in Fig. 2a and b. The SiC particles embedded in the Cu matrix have sizes from ~10 to ~100 µm with a majority of particles having sizes of the order of ~100 µm. In both samples the grain size distributions in the copper matrix are more uniform (Fig. 2c) with an average grain size of ~130 µm. However, some discontinuities are visible in the microstructures, such as the presence of pores in the Cu matrix which appear as white dots in the SE image in Fig. 2d and the lack of bonding between the copper matrix and some SiC particles which are visible as empty spaces on the contact surfaces in Fig. 2d.

The use of HPT processing has a significant impact on the structures of the sintered samples, as illustrated in Figs. 3–5 for Cu, Cu–10SiC and Cu–20SiC samples, respectively. In the pure copper, the HPT processing produces a significant reduction in the pore density. Thus, as can be seen in the SEM image in Fig. 3a, only very fine pores can be identified in the microstructure (marked by arrows). In addition, SEM images taken in orientation contrast mode revealed a significant grain size reduction as shown in Fig. 3b. These grains are relatively equiaxial and with sizes below ~1 µm.

After HPT processing, the microstructures in the samples with the 10% SiC and 20% SiC reinforcements are similar, as shown in Figs. 4 and 5, but there is a significant grain size reduction in the Cu matrix and a decrease in porosity. These SEM observations confirm there is a considerable fragmentation of the SiC particles during the HPT processing (Figs. 4a and 5a). Moreover, the quality of the bonding between the particles and the Cu matrix has improved as is evident in Figs. 4b and Fig. 5b–c. No pores and voids are visible at the interfaces between the SiC particles and the Cu matrix. Nevertheless, the degree of fragmentation appears to be strongly correlated to the original size of the SiC particles. For the largest particles having sizes of ~100 µm, a number of cracks and discontinuities are observed in the Cu–20SiC sample in Fig. 5e. In addition, for most of these particles their outer parts are fragmented into clusters of smaller particles embedded within the Cu matrix and this phenomenon is visible in Fig. 5c and e. At the same time, the fraction of smaller fragmented particles having sizes of ~20–40 µm increased after HPT processing. Some of these particles were fragmented and formed clusters of particles having sizes in the range of ~0.05–1.0 µm (Figs. 4c and 5c). At the same time, a high fraction of fine SiC particles with sizes of ~50–700 nm is found in the Cu matrix (Fig. 5d) where these particles are dispersed in the Cu matrix. Observations by SEM indicate that the fragmentation effect is more intense in the sample with 20% of SiC reinforcement, where there are numerous small particles and clusters of particles in the copper matrix.

The particle sizes were quantitatively analysed in the Cu–10SiC and Cu–20SiC samples and Fig. 6 shows the particles size distributions per unit area for the as-sintered samples (Fig. 6a–c) and HPT-processed

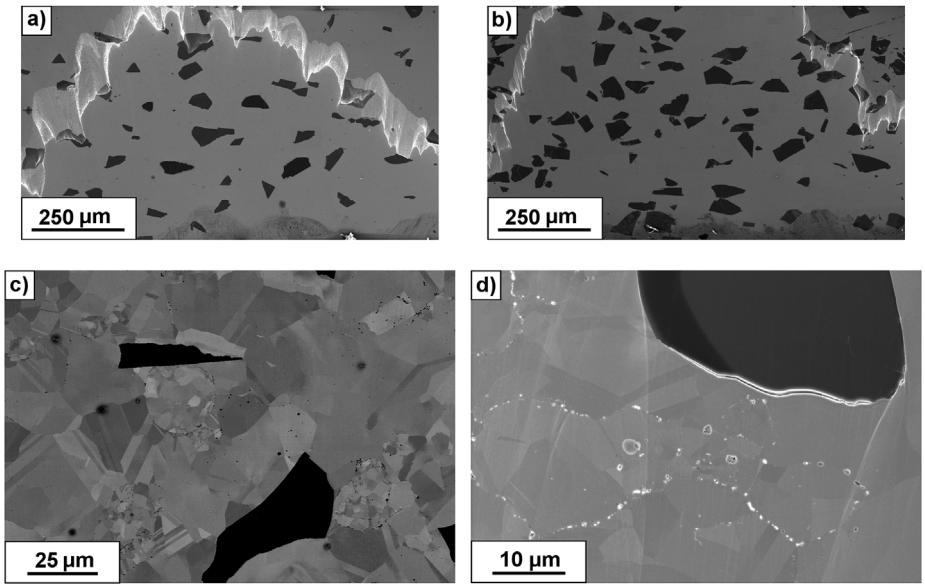

Fig. 2. SEM images of the microstructures of Cu–SiC composites after SPS processing: with 10% (a) at low magnification (c) at high magnification in BSE mode and 20% at (b) low magnification (d) at high magnification in SE mode (the white dots are pores).

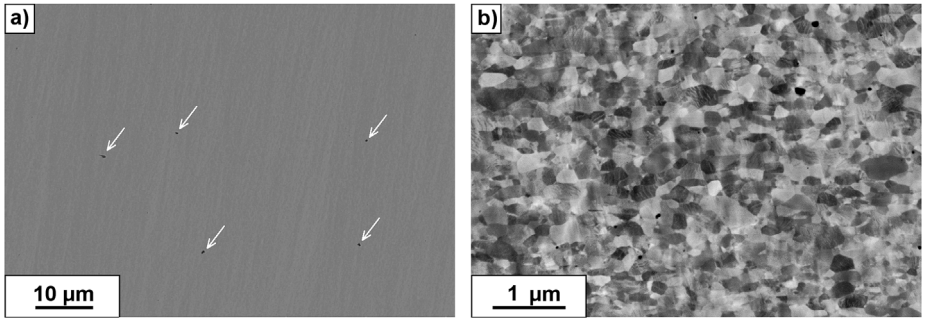

Fig. 3. SEM images of the microstructure of pure Cu after HPT processing.

samples (Fig. 6b–d). In both the Cu–10SiC and Cu–20SiC samples, the numbers of the largest SiC particles after HPT processing decreases when compared with the as-sintered state. At the same time, the fraction of small particles, smaller than 2 μm, increases significantly especially in the sample with 20% of SiC reinforcement where the numbers of particles having sizes in the range of ~50–700 nm reaches ~10^4 per mm^2.

The SEM observations in Figs. 4c and 5d gives clear evidence for grain size refinement in the Cu matrix during HPT processing. However, in order to precisely determine the grain size distributions after HPT processing it was necessary to conduct more detailed investigations. Fig. 7 shows representative STEM images for Cu and the Cu–10SiC and Cu–20SiC samples after HPT processing. The microstructure is generally similar for all samples with the Cu matrix containing both elongated and equiaxial grains with a relatively small density of internal dislocations as shown in Fig. 7 a-c. The average grain size for these conditions was ~360 nm and there were clusters of fragmented SiC particles as in Fig. 7d and undeformed larger particles as in Fig. 7e.

3.2. Mechanical properties

The microhardness distributions across the disc diameters for the SPS-processed samples and samples processed by HPT through 20 turns are presented in Fig. 8. In addition, the average microhardness values with their standard deviations for all samples are given in Table 1. It should be noted that the microhardness measurements were undertaken using a procedure that avoided impinging or hitting any of the large SiC particles with the indenter.

The average microhardness of pure Cu after SPS process is ~58 Hv with a large scatter in the experimental results whereas in the SPS-processed samples with the SiC reinforcement the microhardness of the Cu matrix was at a level of ~65 Hv. After HPT processing, the hardness along the discs diameters in all samples tended to distribute homogenously with only a small depression in the values in the central regions as shown in Fig. 8. In pure Cu, the microhardness increased from ~58 Hv to ~178 Hv. In the samples with the SiC reinforcement, the hardness values were at levels of ~200 Hv and ~230 Hv for the HPT-processed Cu–10SiC and Cu–20SiC samples, respectively. It should be noted that the standard deviation for the SiC-reinforced samples was larger than for the pure Cu sample.

The results of tensile tests for the HPT-processed samples are illustrated in Fig. 9 where these data were complemented with the results for SPS-processed samples. The results and summarised in Table 2 showing the ultimate tensile strength (UTS), yield strength (YS) and elongation to failure. For the sintered Cu material, the YS is at a level of ~130 MPa with a UTS of ~235 MPa. In addition, the material exhibits a large elongation to failure of ~40%. The UTS of samples with the SiC reinforcement is much lower and the values are not larger than ~140 and ~75 MPa for the Cu–10SiC and Cu–20SiC samples, respectively. These samples also exhibited lower elongations to failure with values below 10%.

Processing by HPT has a strong impact on the mechanical behaviour in all samples. Thus, the UTS in pure copper increases from ~235 MPa to ~560 MPa. In the Cu–SiC samples, the UTS increases from ~140 MPa

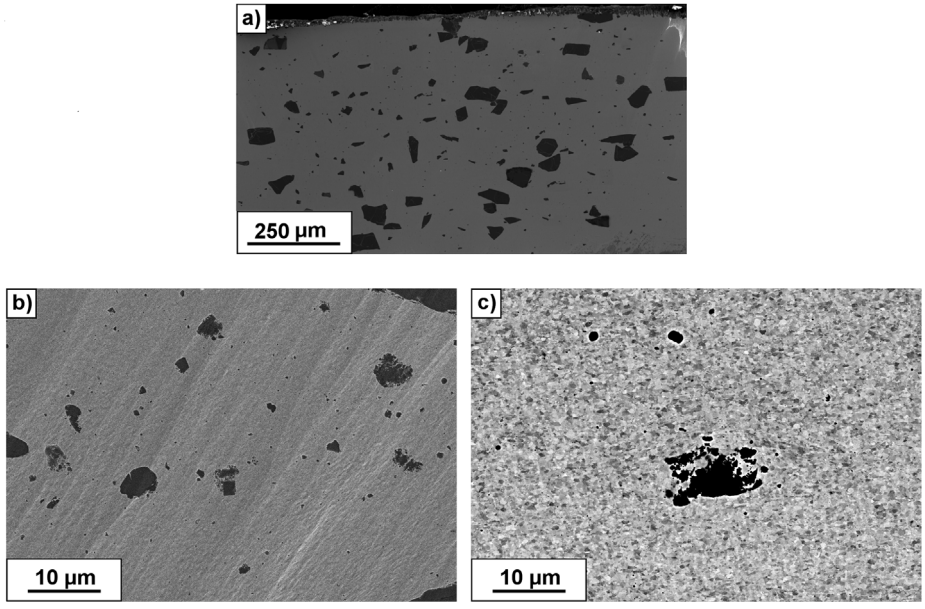

Fig. 4. SEM images of the microstructure of Cu–10SiC composite after HPT processing.

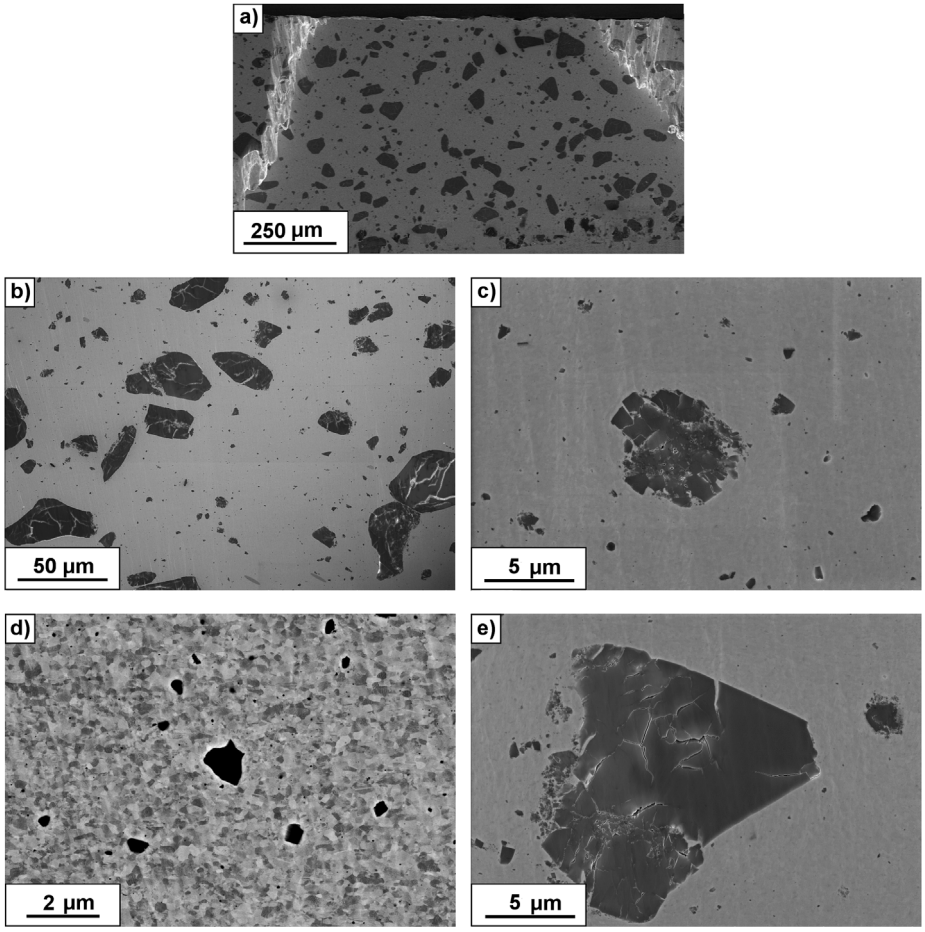

Fig. 5. SEM images of the microstructure of Cu–20SiC composite after HPT processing.

to ~420 MPa in Cu–10SiC and from ~75 MPa to ~440 MPa in Cu–20SiC. This high strength was at the expense of ductility and the elongations to failure dropped to ~10% and ~2% in the pure copper and SiC-reinforced samples, respectively.

3.3. Thermal conductivity

The thermal properties of Cu and the Cu–SiC composites were examined before and after HPT processing. Based on measurements of the thermal diffusivity, the thermal conductivity was estimated and the results are presented in Fig. 10. These data indicate that the fraction volume of SiC and the use of HPT processing have a significant impact on the thermal properties of these materials. The highest values of thermal conductivity were obtained for the SPS-processed copper and HPT-processed copper. As can be seen, the thermal conductivity of the HPT-processed Cu sample, measured at 50 °C, reached a value of ~450 W/mK which is almost 15% higher than the value of ~400 W/mK for the SPS-processed Cu sample. The conductivity values decrease with increasing testing temperature but the observed trend remains visible up to 150 °C. With a testing temperature above 150 °C, the results for the thermal conductivity of SPS-processed Cu and HPT-processed Cu are almost equal at ~375 W/mK.

A similar tendency is observed for the Cu–SiC composite samples. The thermal conductivity of the HPT-processed Cu–10SiC sample, measured at 50 °C, is almost equal to that of pure copper in the SPS state (~385 W/mK). The thermal conductivity values for the SPS-processed and HPT-processed Cu–10SiC samples decrease with increasing testing temperature. In addition, the conductivity values for the HPT-processed samples are higher than for the SPS-processed samples. The largest difference is observed up to 150 °C. At higher temperatures the results are almost equal although the conductivity for the composite samples after HPT processing is always higher by several units.

In the Cu–20SiC samples, the thermal conductivity at 50 °C for the HPT-processed sample is higher than for the SPS-processed sample and it is also higher than for the SPS-processed Cu–10SiC sample. In addition, for both SPS-processed and HPT-processed Cu–20SiC samples the conductivity decreases with increasing temperature but their values never become equal. These thermal conductivity values for the HPT-processed sample are higher by ~100 W/mK at 50 °C and by ~30 W/mK at 300 °C.

4. Discussion

4.1. Microstructures of SPS-processed samples and their evolution during HPT processing

SPS-processed samples exhibit some structural differences depending on their composition. In the pure copper sample the microstructure was highly inhomogeneous in terms of grain size whereas in the Cu–SiC samples the grain size in the copper matrix was more uniform. These structural differences are due to the inhomogeneous recrystallization and grain growth processes occurring during sintering and the inhibition in grain boundary mobility caused by the presence of pores and second phase particles [68,69]. One of the main factors limiting grain growth is the size of the powder particles used in the sintering. Therefore, for pure Cu sample there were large powder particles and it is reasonable to expect significant grain growth. However, a high fraction of fine-grained regions was also observed in this sample and it is worth emphasizing that these refined structures were observed mainly in the regions where there were high densities of pores. Thus,

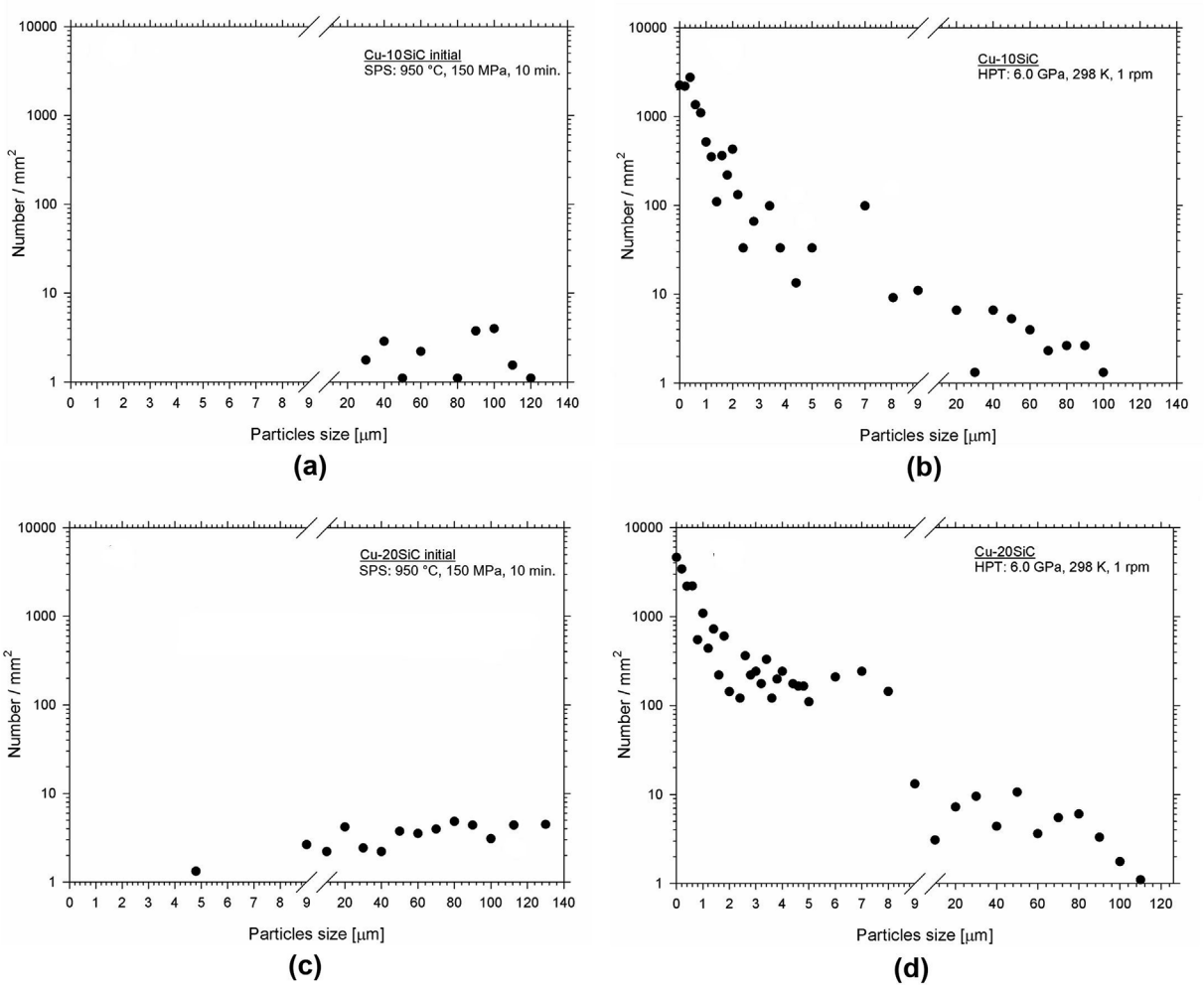

Fig. 6. Particles size distributions in Cu–SiC samples after SPS processing (a, c) and after HPT processing (b, d).

the presence of porosity significantly inhibits diffusion and grain growth by reducing the diffusion area [68,69]. Moreover, the surface area of the powder particles is always slightly oxidized and this oxidation also inhibits grain growth. Both factors play a significant role in the formation of fine-grained structures in the copper sample.

The addition of SiC particles acts to homogenise the grain size distribution in the Cu matrix. The SiC particles are thermally stable elements and they play a role as barriers impeding grain growth and recrystallization processes [70,71]. The inhibition of grain growth by dispersed particles, combined with the effects resulting from residual porosity and oxidation, leads to a more homogeneous average grain size in the copper matrix. In addition, it is worth noting that there were numerous discontinuities and voids at the interface between the SiC particles and the Cu matrix in these samples and this indicates that the SiC particles exhibit a poor wettability during sintering.

The results show also that HPT processing of Cu and Cu–SiC composites produces significant changes in the microstructure.

Firstly, it has a beneficial influence on the reduction of residual porosity. The SEM images in Fig. 3 show the presence of only single pores in all microstructures and no voids were observed at the interfaces between the SiC particles and the Cu matrix after HPT processing. The closure of pores is related to the processing parameters and is a direct consequence of the high imposed compressive pressure of 6.0 GPa and the high shear strains of more than ~400 generated in the outer parts of the discs during HPT. Both factors contribute to the closure of the remaining voids and pores in the samples [62,72,73] leading to further densification.

Secondly, the HPT processing causes a significant grain refinement in pure copper and the copper matrix as in Figs. 3–4 and the average grain size in all samples was of the order of ~360 nm. This is similar to the grain size in pure copper after 10 HPT revolutions which was reported as ~300 nm [74].

Thirdly, the HPT processing has a dual effect on the evolution of SiC particles in the composite samples. It leads to a significant fragmentation of the SiC particles as confirmed by SEM observations (Figs. 4 and 5) and quantitative analysis (Fig. 6). The number density of large SiC particles decreased and the number density of nanometric fragmented SiC particles significantly increased. In addition, after a large number of HPT turns there was a homogeneous distribution of fragmented SiC particles in the Cu matrix. A fragmentation of the hard ceramic phase during SPD processing was reported earlier for various MMCs, such as ZnO in a Cu matrix [73], Al_2O_3 in an aluminium matrix [75,76], SiC in an Al matrix [76], Al_3Ti in an aluminium matrix [77], TiB in Al and Ti matrices [78,79] and SiC in a Cu matrix [62]. These various reports demonstrate that the combination of a high compressive pressure with the high shear strains generated during torsional straining in HPT and the low fracture toughness of the SiC reinforcing phase favours particle fragmentation during processing [62,80]. The SiC ceramic particles embedded in the Cu matrix undergo an unusually high extent of plastic deformation during the HPT processing. Thus, extremely high shear strains are generated during HPT and this promotes dislocation formation in the ceramic phase (Fig. 7e), an activation of their movement by slip and then facilitates the transformation of slip bands to microcracks causing the fragmentation of the ceramic phase [62,80].

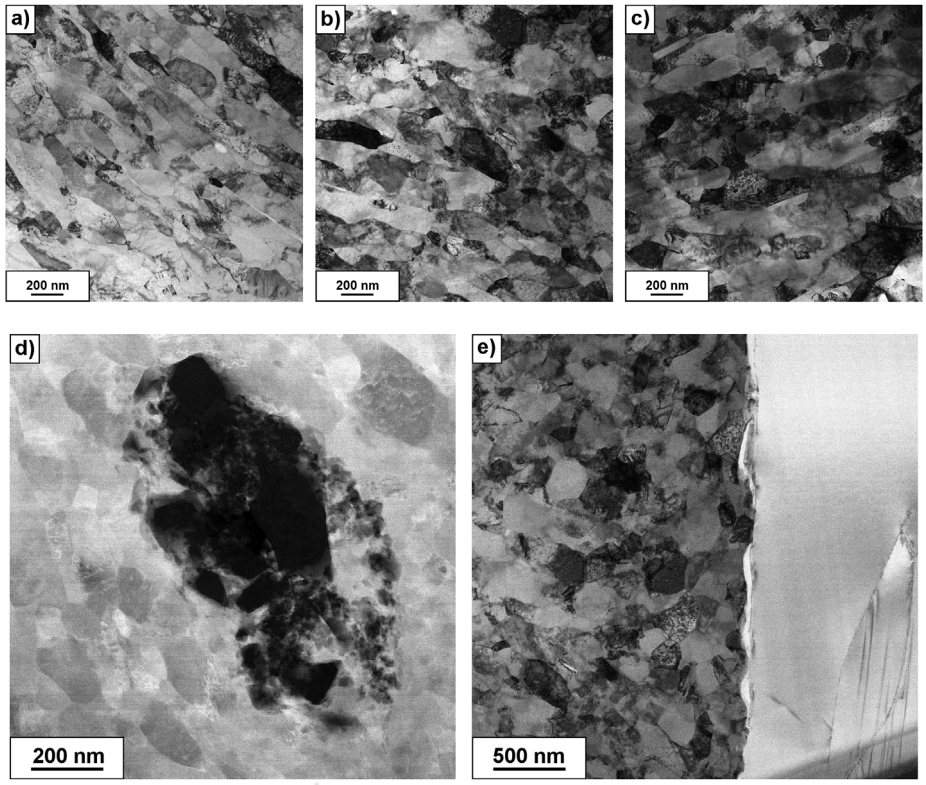

Fig. 7. STEM images of the Cu–SiC microstructure after HPT processing: (a) pure Cu, (b) Cu10SiC, (c) Cu20SiC, (d) a cluster of fine SiC particles embedded in Cu matrix, (e) interface between big SiC particle and Cu matrix.

It is worth emphasizing that the fragmentation effects reported in these experiments were not fully completed and high numbers of large SiC particles were observed in the microstructures after HPT processing (Figs. 4–6) which are a consequence of the insufficient strain that was imposed during HPT processing. Moreover, most of these particles contained numerous cracks and voids. By contrast, it was demonstrated that the size of SiC particles may be drastically reduced after 15 HPT revolutions [62] but in those studies powder particles were smaller than ~30 μm and therefore easier to fragment. These experiments also employed a higher compressive pressure of 10 GPa which again favours the formation of higher stresses in the material.

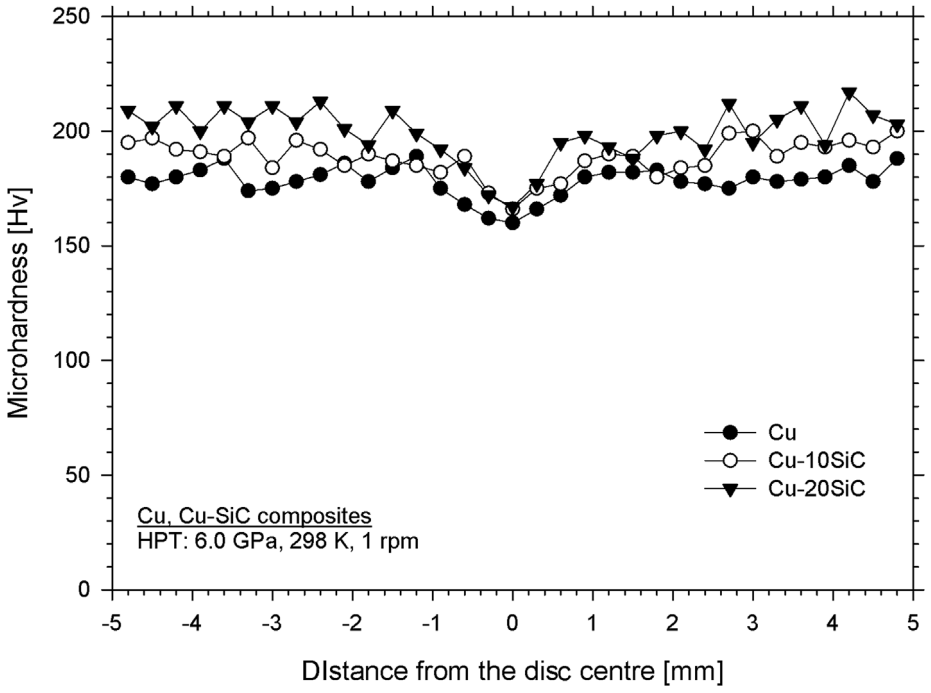

Fig. 8. Variations of hardness with distance from the disc centre for Cu and Cu–SiC samples after HPT processing.

Table 1
Showing average microhardness of studied samples together with their standard deviation.

Sample	Microhardness	Standard deviation
Cu sintered	58	7.6
Cu–10SiC sintered	65	3.4
Cu–20SiC sintered	66	2.5
Cu HPT	178	6.7
Cu–10SiC HPT	199	7.9
Cu–20SiC HPT	228	13.1

Table 2
Mechanical properties determined in tensile tests.

Sample	UTS [MPa]	YS [MPa]	Elongation [%]
Cu sintered	235	130	40
Cu–10SiC sintered	140	110	9
Cu–20SiC sintered	75	68	2.3
Cu HPT	560	480	10.3
Cu–10SiC HPT	440	395	2.9
Cu–20SiC HPT	420	385	1.9

4.2. The effect of HPT processing on the mechanical properties

The experimental results in these experiments prove that a combination of SPS and HPT processing is effective in producing MMC samples with exceptionally high strength. The SPS samples exhibited significant differences in the microhardness results with ~58 Hv and high scatter for pure copper and ~65 Hv for the MMCs with 10% and 20% of SiC reinforcement. The observed differences are related to the microstructures of these samples. Thus, in the pure copper sample a high grain size inhomogeneity was observed and this gave a reduced hardness and a large scatter in the experimental results. In the MMCs samples, where the SiC particles inhibited grain growth, the microstructure was homogeneous in terms of grain size and the hardness values were higher and more uniform.

In the samples processed by HPT, the microhardness increased more than three times and there was a reasonable level of homogeneity throughout the disc with only a small drop in hardness in the central regions. This indicates that the materials reached a saturation state [81]. After HPT processing, the average microhardness values increased to ~178 Hv for pure Cu and ~200 Hv and ~230 Hv for Cu–10SiC and Cu–20SiC, respectively. Such an increase in microhardness after HPT processing is related to the grain refinement in the Cu matrix, the increased density of dislocations and, for the MMCs, with the presence of fragmented fine SiC particles which act as obstacles to dislocation motion according to the Orowan model [82]. The fragmentation of the ceramic phase generates a high fraction of homogeneously distributed SiC nano-particles, as shown by the microstructure images presented in Figs. 4–5 and the particle size distributions in Fig. 6. The fragmentation of SiC particles is more intense for the sample containing 20% of reinforcement and this leads to the higher microhardness values in this sample.

The presence of an SiC reinforcement also has a major impact on the mechanical properties as measured in the tensile testing. In the SPS samples, the highest strength was obtained for pure copper (~200 MPa) whereas in the Cu–10SiC and Cu–20SiC samples the UTS values were ~130 MPa and ~75 MPa, respectively. This large reduction in strength is attributed to the presence of numerous pores and discontinuities at the interfaces between the Cu matrix and the SiC particles, as visible in Figs. 1 and 2, which act as stress concentrators leading to the propagation of cracks [83] and giving material failure at lower stresses. These results are consistent with earlier studies on Cu–SiC composites fabricated by various powder metallurgy techniques [15,26]. The poor wettability of SiC by copper significantly reduces the strength of the sintered samples [84].

The samples processed by HPT exhibited higher strength than those of the coarse-grained materials. The improvement in UTS of the pure Cu and Cu–SiC samples is associated with matrix strengthening through the grain refinement according to the Hall–Petch relationship [85,86]. In addition, the increased number density of fragmented nano-sized SiC particles [14,62] also plays a beneficial role contributing to the increase in the UTS. In earlier work a UTS as high as 850 MPa was reported for Cu–20SiC after 15 HPT revolutions [62]. However, the SiC particles used in the earlier experiments were smaller and therefore easier to fragment whereas the SiC particles in this study had diameters of ~100 μm. As presented in the SEM images in Figs. 4 and 5, even 20 HPT

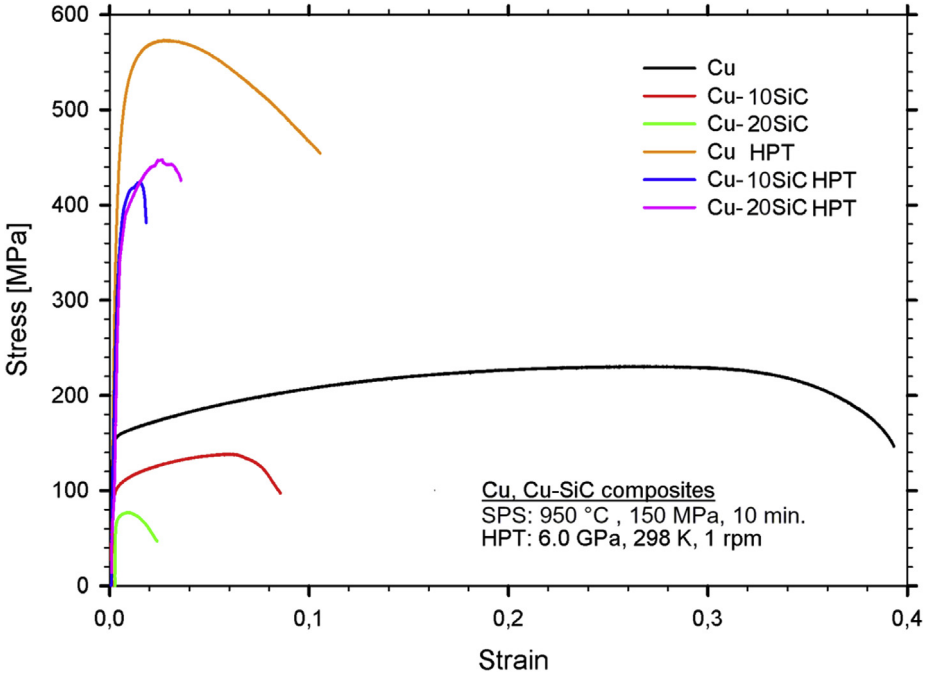

Fig. 9. Plots of stress versus strain for tensile specimens processed by HPT.

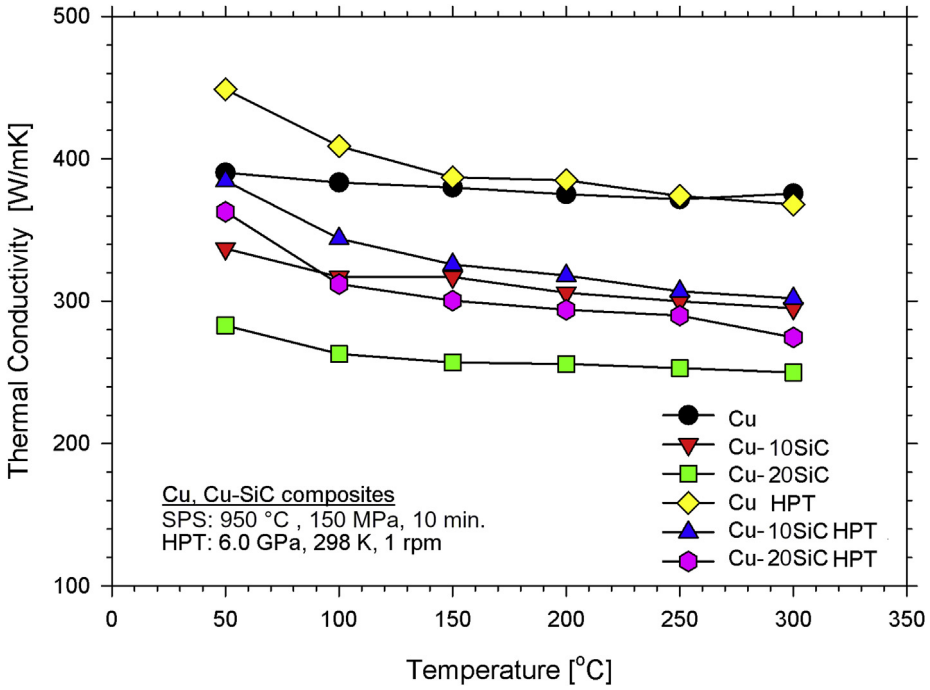

Fig. 10. Thermal conductivity as a function of temperature for SPS-processed samples and HPT-processed samples.

revolutions under a pressure of 6.0 GPa failed to produce sufficient shear forces to fully fragment such large particles (Fig. 6). Moreover, after HPT processing most of the remaining large particles were cracked (Fig. 5) which may also have a negative effect on the strength [83].

4.3. Effect of plastic deformation on thermal conductivity

No data on the effect of HPT on the thermal conductivity of Cu and Cu–SiC composites were reported so far. Therefore, it is important to provide a basic explanation of the thermal conductivity changes observed in Fig. 10. The results clearly show that the high plastic deformation introduced during HPT processing enhances the thermal conductivity. Thus, its value for pure copper subjected to 20 turns of HPT was ~445 W/(mK) while the thermal conductivity of sintered copper was only ~390 W/(mK). The results for the Cu–SiC MMCs are lower than those for the pure metal which is reasonable since the conductivity of SiC is 360 W/(mK). However, even in these samples there was an observable increase in the conductivity after HPT processing. Several factors may be responsible for this behaviour.

The first factor is associated with the further densification of the sample during HPT processing. The pores and other discontinuities are structural barriers to heat flow. Therefore, intense plastic deformation closes most of these defects, as in Figs. 3–5, thereby increasing the thermal conductivity.

The second factor is associated with structural changes in the Cu matrix. A large amount of cold working makes the samples thermally unstable and the rate of heat emission is enhanced [87,88]. As a consequence of plastic deformation and residual stresses, the lattice parameter may be slightly changed. Thus, atoms are more densely packed and the heat transfer is enhanced by physical or atomic contact between the conducting atoms. As a result, the absorbed heat is quickly transferred from one atom to the other [89,90]. It is also worth examining the density of defects generated during the SPD processing. In general, all structural defects are considered as structural barriers for heat flow. Some investigations suggest that dislocations are a source of anharmonic phonon–phonon scattering and this reduces the relaxation time of longitudinal acoustic phonons [91]. Increased phonon scattering by dislocations has been suggested as an explanation for the thermal conductivity reduction [91,92]. At some point, the numbers of scattering dislocations may be reduced due to dislocation annihilation [81]. Pure metals, such as the 99.99Cu used in this study, have a strong tendency for recovery processes and the density of defects is lower than in their alloys. This means that the effect of dislocation scattering on the thermal properties is probably essentially negligible.

5. Summary and conclusions

1) Samples of Cu, Cu–10SiC and Cu–20SiC were successfully consolidated by the SPS technique. Nevertheless, pores and voids remained at the interfaces between the Cu matrix and the SiC particles. Further processing by HPT made it possible to substantially reduce the residual porosity as well as increasing the bonding between the Cu matrix and the SiC particles.
2) Processing by HPT with a pressure of 6.0 GPa and 20 revolutions produced an ultrafine-grained structure in the Cu matrix for all samples with an average grain size of ~360 nm. It also led to the fragmentation of the SiC phase. As a result, high numbers of nano-sized SiC particles were observed after processing.
3) The presence of SiC nanoparticles and a refined microstructure in the Cu matrix contributed to an increase in the microhardness in the Cu and Cu–SiC samples.
4) The use of HPT processing significantly improves the strength of Cu–SiC composites but the presence of some remaining cracked large SiC particles had a negative impact on the strength of the MMCs which remained not higher than ~450 MPa.
5) It is shown that the thermal conductivity of Cu-based MMCs may be enhanced by subjecting these samples to intensive plastic deformation.

Acknowledgments

The work was supported by the National Science Centre, Poland, within the project SONATINA 1 “Synthesis of novel hybrid materials using High-Pressure Torsion”, under Grant Agreement No. UMO-2017/24/C/ST8/00145.

References

[1] W. Bai, A. Roy, R. Sun, V.V. Silberschmidt, Enhanced machinability of SiC-reinforced metal-matrix composite with hybrid turning, J. Mater. Process. Technol. 268 (2019) 149–161 https://doi.org/10.1016/j.jmatprotec.2019.01.017.

[2] J. Lin, K. Ma, H. Yang, M. Li, E.J. Lavernia, J.M. Schoenung, The microstructural design of trimodal aluminum composites, JOM 66 (2014) 898–908 https://doi.org/10.1007/s11837-014-0906-2.

[3] Ri. Gecu, Y. Yurekturk, E. Tekoglu, F. Muhaffel, A. Karaaslan, Improving wear resistance of 304 stainless steel reinforced AA7075 aluminum matrix composite by micro-arc oxidation, Surf. Coat. Technol. 368 (2019) 15–24 https://doi.org/10.1016/j.surfcoat.2019.04.029.

[4] B. Jin, D.-B. Xiong, Zhanqiu Tan, G. Fan, D. Zhang, Enhanced corrosion resistance in metal matrix composites assembled from graphene encapsulated copper nanoflakes, Carbon 142 (2019) 482–490 https://doi.org/10.1016/j.carbon.2018.10.088.

[5] S. Sivakumar, S.K. Thimmappa, B.R. Golla, Corrosion behavior of extremely hard Al-Cu/Mg-SiC light metal alloy composites, J. Alloy. Comp. 767 (2018) 703–711 https://doi.org/10.1016/j.jallcom.2018.07.117.

[6] R. Venkatesh, V.S. Rao, Thermal, corrosion and wear analysis of copper based metal matrix composites reinforced with alumina and graphite, Def Technol. 14 (2018) 346–355 https://doi.org/10.1016/j.dt.2018.05.003.

[7] K.E. Pappacena, M.T. Johnson, H. Wang, W.D. Porter, K.T. Faber, Thermal properties of wood-derived copper–silicon carbide composites fabricated via electrodeposition, Compos. Sci. Technol. 70 (2010) 478–484 https://doi.org/10.1016/j.compscitech.2009.11.011.

[8] M. Barmouz, M.K.B. Givi, Fabrication of in situ Cu/SiC composites using multi-pass friction stir processing: evaluation of microstructural, porosity, mechanical and electrical behaviour, Compos. Part A 42 (2011) 1445–1453 https://doi.org/10.1016/j.compositesa.2011.06.010.

[9] Z. Liao, A. Abdelhafeez, H. Li, Y. Yang, D. Axinte, State-of-the-art of surface integrity in machining of metal matrix composites, Int. J. Mach. Tool Manuf. 143 (2019) 63–91 https://doi.org/10.1016/j.ijmachtools.2019.05.006.

[10] G. Sdanghi, G. Maranzana, A. Celzard, V. Fierro, Review of the current technologies and performances of hydrogen compression for stationary and automotive applications, Renew. Sustain. Energy Rev. 102 (2019) 150–170 https://doi.org/10.1016/j.rser.2018.11.028.

[11] F. Shehata, A. Fathy, M. Abdelhameed, S.F. Moustafa, Preparation and properties of Al2O3 nanoparticle reinforced copper matrix composites by in situ processing, Mater. Des. 30 (2009) 2756–2762 https://doi.org/10.1016/j.matdes.2008.10.005.

[12] S.F. Moustafa, Z. Abbel-Hamid, A.M. Abd-Elhay, Copper matrix SiC and Al2O3 particulate composites by powder metallurgy technique, Mater. Lett. 53 (2002) 244–249 https://doi.org/10.1016/S0167-577X(01)00485-2.

[13] M. López, D. Corredor, C. Camurri, V. Vergara, J. Jiménez, Performance and characterization of dispersion strengthened Cu–TiB2 composite for electrical use, Mater. Char. 55 (2005) 252–262 https://doi.org/10.1016/j.matchar.2005.04.006.

[14] M.R. Akbarpour, E. Salahi, F. Alikhani Hesari, E.Y. Yoon, H.S. Kim, A. Simchi, Microstructural development and mechanical properties of nanostructured copper reinforced with SiC nanoparticle, Mater. Sci. Eng. A 568 (2013) 33–39 https://doi.org/10.1016/j.msea.2013.01.010.

[15] M. Chmielewski, K. Pietrzak, A. Strojny-Nędza, K. Kaszyca, R. Zybała, P. Bazarnik, M. Lewandowska, S. Nosewicz, Microstructure and thermal properties of Cu-SiC composite materials depending on the sintering technique, Sci. Sinter. 49 (2017) 11–22 https://doi.org/10.2298/SOS1701011C.

[16] S.T.K. Rajan, A.N. Balaji, P. Narayanasamy, S.C. Vettivel, Microstructural, electrical, thermal and tribological studies of copper-fly ash composites through powder metallurgy, Bull. Pol. Acad.: Technol. 66 (2018) 935–940 https://doi.org/10.24425/bpas.2018.125941.

[17] G.C. Efe, I. Altinsoy, M. Ipek, S. Zeytin, C. Bindal, Effects of SiC on properties of Cu-SiC metal matrix composites, AIP Conf. Proc. 1400 (2011) 529–534 https://doi.org/10.1063/1.3663176.

[18] A. Ramanathan, P.K. Krishnan, R. Muraliraja, A review on the production of metal matrix composites through stir casting – furnace design, properties, challenges, and research opportunities, J. Manuf. Process. 42 (2019) 213–245 https://doi.org/10.1016/j.jmapro.2019.04.017.

[19] B.C. Kandpal, J. Kumar, H. Singh, Manufacturing and technological challenges in Stir casting of metal matrix composites– A review, Mater. Today Proc. 5 (2018) 5–10 https://doi.org/10.1016/j.matpr.2017.01.130.

[20] T.S. Srivatsan, E.J. Lavernia, Use of spray techniques to synthesize particulate-reinforced metal-matrix composites, J. Mater. Sci. 27 (1992) 5965–5981, https://doi.org/10.1007/BF01133739.

[21] J. Maj, M. Basista, W. Węglewski, K. Bochenek, A. Strojny-Nędza, K. Naplocha, T. Panzner, M. Tatarková, F. Fiori, Effect of microstructure on mechanical properties and residual stresses in interpenetrating aluminum-alumina composites fabricated by squeeze casting, Mater. Sci. Eng. A 715 (2018) 154–162, https://doi.org/10.1016/j.msea.2017.12.091.

[22] D. Apelian, Particulate Processing (Powder Metallurgy), Encyclopedia of Materials: Science and Technology, second ed., Elsevier, Pergamon, 2001, pp. 6761–6768 https://doi.org/10.1016/B0-08-043152-6/01197-9.

[23] N.P. Hung, C.S. Lim, Y.K. Ho, Y.C. Tan, W.G. Tan, Cumulative creep and hot isostatic pressing of particle-reinforced metal matrix composites, J. Mater. Process. Technol. 101 (2000) 104–109 https://doi.org/10.1016/S0924-0136(00)00399-X.

[24] G. Miranda, A. Araújo, F. Bartolomeu, M. Buciumeanu, O. Carvalho, J.C.M. Souza, F.S. Silva, B. Henriques, Design of Ti6Al4V-HA composites produced by hot pressing for biomedical applications, Mater. Des. 108 (2016) 488–493 https://doi.org/10.1016/j.matdes.2016.07.023.

[25] M. Razavi, A.R. Farajipour, M. Zakeri, M.R. Rahimipour, A.R. Firouzbakht, Production of Al2O3–SiC nano-composites by spark plasma sintering, Boletín La Soc Española Cerámica Y Vidr 56 (2017) 186–194, https://doi.org/10.1016/j.bsecv.2017.01.002.

[26] M. Chmielewski, S. Nosewicz, E. Wyszkowska, Ł. Kurpaska, A. Strojny-Nędza, A. Piątkowska, P. Bazarnik, K. Pietrzak, Analysis of the micromechanical properties of copper-silicon carbide composites using nanoindentation measurements, Ceram. Int. 45 (2019) 9164–9173 https://doi.org/10.1016/j.ceramint.2019.01.257.

[27] M.J. Tan, X. Zhang, Powder metal matrix composites: selection and processing, Mater. Sci. Eng. A 244 (1998) 80–85 https://doi.org/10.1016/S0921-5093(97)00829-0.

[28] I. Sabirov, O. Kolednik, R.Z. Valiev, R. Pippan, Equal channel angular pressing of metal matrix composites: effect on particle distribution and fracture toughness, Acta Mater. 53 (2005) 4919–4930 https://doi.org/10.1016/j.actamat.2005.07.010.

[29] I. Sabirov, O. Kolednik, R. Pippan, Homogenization of metal matrix composites by high-pressure torsion, Metall. Mater. Trans. A 36 (2005) 2861–2870 https://doi.org/10.1007/s11661-005-0281-2.

[30] Y. Huang, P. Bazarnik, D. Wan, D. Luo, P.H.R. Pereira, M. Lewandowska, J. Yao, B.E. Hayden, T.G. Langdon, The fabrication of graphene-reinforced Al-based nanocomposites using high-pressure torsion, Acta Mater. 164 (2019) 499–511 https://doi.org/10.1016/j.actamat.2018.10.060.

[31] S.N. Alhajeri, K.J. Al-Fadhalah, A.I. Almazrouee, T.G. Langdon, Microstructure and microhardness of an Al-6061 metal matrix composite processed by high-pressure torsion, Mater. Char. 118 (2016) 270–278 https://doi.org/10.1016/j.matchar.2016.06.003.

[32] M. Kawasaki, Y. Huang, C. Xu, M. Furukawa, Z. Horita, T.G. Langdon, A quantitative study of cavity development in the tensile testing of an aluminum metal matrix composite processed by equal-channel angular pressing, Mater. Sci. Eng. A 410–411 (2005) 402–407.

[33] D. Ma, J. Wang, K. Xu, Equal channel angular pressing of a SiCw reinforced aluminum-based composite, Mater. Lett. 56 (2002) 999–1002, https://doi.org/10.1016/S0167-577X(02)00662-6.

[34] B.Q. Han, T.G. Langdon, Achieving enhanced tensile ductility in an Al-6061 composite processed by severe plastic deformation, Mater. Sci. Eng. A 410–411 (2005) 430–434.

[35] M.A. Muñoz-Morris, N. Calderón, I. Gutierrez-Urrutia, D.G. Morris, Matrix grain refinement in Al–TiAl composites by severe plastic deformation: influence of particle size and processing route, Mater. Sci. Eng. A 425 (2006) 131–137.

[36] G. Ramu, R. Bauri, Effect of equal channel angular pressing (ECAP) on microstructure and properties of Al–SiCp composites, Mater. Des. 30 (2009) 3554–3559.

[37] L. Bian, W. Liang, G. Xie, W. Zhang, J. Xue, Enhanced ductility in an Al–Mg2Si in situ composite processed by ECAP using a modified BC route, Mater. Sci. Eng. A 528 (2011) 3463–3467.

[38] I. Sabirov, R. Pippan, Formation of a W–25% Cu nanocomposite during high pressure torsion, Scr. Mater. 52 (2005) 1293–1298.

[39] X. Sauvage, R. Pippan, Nanoscaled structure of a Cu–Fe composite processed by high-pressure torsion, Mater. Sci. Eng. A 410–411 (2005) 345–347.

[40] I. Sabirov, R. Pippan, Characterization of tungsten fragmentation in a W–25% Cu composite after high-pressure torsion, Mater. Char. 58 (2007) 848–853.

[41] X. Quelennec, A. Menand, J.M. Le Breton, R. Pippan, X. Sauvage, Homogeneous Cu–Fe supersaturated solid solutions prepared by severe plastic deformation, Philos. Mag. 90 (2010) 1179–1195.

[42] Y.Z. Tian, Z.F. Zhang, T.G. Langdon, Achieving homogeneity in a two-phase Cu–Ag composite during high-pressure torsion, J. Mater. Sci. 48 (2013) 4606–4612.

[43] C. Gode, H. Yilmazer, I. Ozdemir, Y. Todaka, Microstructural refinement and wear property of Al–Si–Cu composite subjected to extrusion and high-pressure torsion, Mater. Sci. Eng. A 618 (2014) 377–384.

[44] M.R. Akbarpour, M. Farvizi, D.J. Lee, H. Rezaei, H.S. Kim, Effect of high-pressure torsion on the microstructure and strengthening mechanisms of hot-consolidated Cu–CNT nanocomposite, Mater. Sci. Eng. A 638 (2015) 289–295.

[45] S. Sabbaghianrad, T.G. Langdon, Developing superplasticity in an aluminum matrix composite processed by high-pressure torsion, Mater. Sci. Eng. A 655 (2016) 36–43 https://doi.org/10.1016/j.msea.2015.12.078.

[46] A.P. Zhilyaev, T.G. Langdon, Using high-pressure torsion for metal processing: fundamentals and applications, Prog. Mater. Sci. 53 (2008) 893–979.

[47] R.Z. Valiev, T.G. Langdon, Principles of equal-channel angular pressing as a processing tool for grain refinement, Prog. Mater. Sci. 51 (2006) 881–981.

[48] Y. Saito, H. Utsunomiya, N. Tsuji, T. Sakai, Novel ultra-high straining process for bulk materials—development of the accumulative roll-bonding (ARB) process, Acta Mater. 47 (1999) 579–583 https://doi.org/10.1016/S1359-6454(98)00365-6.

[49] M. Lewandowska, H. Garbacz, W. Pachla, K.J. Kurzydlowski, Hydrostatic extrusion and nanostructure formation in an aluminium alloy, Solid State Phenom. 101–102 (2005) 65–69.

[50] P. Bazarnik, M. Lewandowska, K.J. Kurzydlowsk, Mechanical behaviour of ultrafine grained AI-Mg alloys obtained by different processing routes, Arch. Metall. Mater. 57 (2012) 869–876, https://doi.org/10.2478/V10172-012-0096-2.

[51] P. Bazarnik, Y. Huang, M. Lewandowska, T.G. Langdon, Structural impact on the Hall–Petch relationship in an Al–5Mg alloy processed by high-pressure torsion, Mater. Sci. Eng. A 626 (2015) 9–15 https://doi.org/10.1016/j.msea.2014.12.027.

[52] A.T. Krawczynska, S. Gierlotka, P. Suchecki, D. Setman, B. Adamczyk-Cieslak, M. Gloc, W. Chrominski, M. Lewandowska, M. Zehetbauer, Phenomena occurring in nanostructured stainless steel 316LVM during annealing under high hydrostatic pressure, Adv. Eng. Mater. 21 (2019) 1800101 https://doi.org/10.1002/adem.201800101.

[53] V.V. Stolyarov, Y.T. Zhu, T.C. Lowe, R.K. Islamgaliev, R.Z. Valiev, Processing nanocrystalline Ti and its nanocomposites from micrometer-sized Ti powder using

high pressure torsion, Mater. Sci. Eng. A 282 (2000) 78–85 https://doi.org/10.1016/S0921-5093(99)00764-9.
[54] A.P. Zhilyaev, G. Ringot, Y. Huang, J.M. Cabrera, T.G. Langdon, Mechanical behavior and microstructure properties of titanium powder consolidated by high-pressure torsion, Mater. Sci. Eng. A 688 (2017) 498–504 https://doi.org/10.1016/j.msea.2017.02.032.
[55] S. Sabbaghianrad, M. Kawasaki, T.G. Langdon, Microstructural evolution and the mechanical properties of an aluminum alloy processed by high-pressure torsion, J. Mater. Sci. 47 (2012) 7789–7795.
[56] A.P. Zhilyaev, A.A. Gimazov, G.I. Raab, T.G. Langdon, Using high-pressure torsion for the cold-consolidation of copper chips produced by machining, Mater. Sci. Eng. A 486 (2008) 123–126.
[57] M.M. de Castro, A.P. Carvalho, P.H.R. Pereira, A.C. Isaac Neta, R.B. Figueiredo, T.G. Langdon, Consolidation of magnesium and magnesium alloy machne chips using high-pressure torsion, Mater. Sci. Forum 941 (2018) 851–856.
[58] J.-K. Han, X. Li, R. Dippenaar, K.-D. Liss, M. Kawasaki, Microscopic plastic response in a bulk nano-structured TiAl intermetallic compound processed by high-pressure torsion, Mater. Sci. Eng. A 714 (2018) 84–92 https://doi.org/10.1016/j.msea.2017.12.065.
[59] K. Edalati, S. Toh, M. Watanabe, Z. Horita, In situ production of bulk intermetallic-based nanocomposites and nanostructured intermetallics by high-pressure torsion, Scr. Mater. 66 (2012) 386–389 https://doi.org/10.1016/j.scriptamat.2011.11.039.
[60] M.M. Castro, P.H.R. Pereira, A. Isaac, R.B. Figueiredo, T.G. Langdon, Development of a magnesium/alumina composite through cold consolidation of machining chips by high-pressure torsion, J. Alloy. Comp. 780 (2019) 422–427.
[61] M.M. Castro, S. Sabbaghianrad, P.H.R. Pereira, E.M. Mazzer, A. Isaac, T.G. Langdon, R.B. Figueiredo, A magnesium-aluminium composite produced by high-pressure torsion, J. Alloy. Comp. 804 (2019) 421–426.
[62] M.I.A. El Aal, Effect of high-pressure torsion processing on the microstructure evolution and mechanical properties of consolidated micro size Cu and Cu-SiC powders, Adv. Powder Technol. 28 (2017) 2135–2150 https://doi.org/10.1016/j.apt.2017.05.020.
[63] O. Ghaderi, M.R. Toroghinejad, A. Najafizadeh, Investigation of microstructure and mechanical properties of Cu–SiCP composite produced by continual annealing and roll-bonding process, Mater. Sci. Eng. A 565 (2013) 243–249 https://doi.org/10.1016/j.msea.2012.11.004.
[64] M. Jahedi, M.H. Paydar, M. Knezevic, Enhanced microstructural homogeneity in metal-matrix composites developed under high-pressure-double-torsion, Mater. Char. 104 (2015) 92–100 https://doi.org/10.1016/j.matchar.2015.04.012.
[65] R.B. Figueiredo, P.R. Cetlin, T.G. Langdon, Using finite element modelling to examine the flow processes in quasi-constrained high-pressure torsion, Mater. Sci. Eng. A 528 (2011) 8198–8204.
[66] R.M. Molak, K. Paradowski, T. Brynk, L. Ciupinski, Z. Pakiela, K.J. Kurzydlowski, Measurement of mechanical properties in a 316L stainless steel welded joint, Int. J. Press. Vessel. Pip. 86 (2009) 43–47.
[67] S. Min, J. Blumm, A. Lindemann, A new laser flash method for measurement of the thermophysical properties, Thermochim. Acta 455 (2007) 46–49.
[68] N.A. Rawashdeh, W. Khraisat, H. Borgström, Pinning effect of pores on grain growth in sintered steel, Jordan J. Mech. Ind. Eng. 11 (2017) 73–78.
[69] V. Rehn, J. Hötzer, W. Rheinheimer, M. Seiz, C. Serr, B. Nestler, Phase-field study of grain growth in porous polycrystals, Acta Mater. 174 (2019) 439–449 https://doi.org/10.1016/j.actamat.2019.05.059.
[70] S. Farag, I. Konyashin, B. Ries, The influence of grain growth inhibitors on the microstructure and properties of submicron, ultrafine and nano-structured hard-metals – a review, Int. J. Refract. Metals Hard 77 (2018) 12–30 https://doi.org/10.1016/j.ijrmhm.2018.07.003.
[71] M. Ao, H. Liu, C. Dong, The effect of La2O3 addition on intermetallic-free aluminium matrix composites reinforced with TiC and Al2O3 ceramic particles, Ceram. Int. 45 (2019) 12001–12009 https://doi.org/10.1016/j.ceramint.2019.03.093.
[72] Y. Qi, A. Kosinova, A.R. Kilmametov, B.B. Straumal, E. Rabkin, Generation and healing of porosity in high purity copper by high-pressure torsion, Mater. Char. 145 (2018) 1–9 https://doi.org/10.1016/j.matchar.2018.08.023.
[73] Y. Qi, A. Kosinova, A.R. Kilmametov, B.B. Straumal, E. Rabkin, Plastic flow and microstructural instabilities during high-pressure torsion of Cu/ZnO composites, Mater. Char. 145 (2018) 389–401 https://doi.org/10.1016/j.matchar.2018.09.001.
[74] Z. Horita, T.G. Langdon, Microstructures and microhardness of an aluminum alloy and pure copper after processing by high-pressure torsion, Mater. Sci. Eng. A 410–411 (2005) 422–425 https://doi.org/10.1016/j.msea.2005.08.133.
[75] K. Edalati, M. Ashida, Z. Horita, T. Matsui, H. Kato, Wear resistance and tribological features of pure aluminum and Al–Al2O3 composites consolidated by high-pressure torsion, Wear 310 (2014) 83–89 https://doi.org/10.1016/j.wear.2013.12.022.
[76] K.C. Nayak, P.P. Date, Hot deformation flow behavior of powder metallurgy based Al-SiC and Al-Al2O3 composite in a single step and two-step uni-axial compression, Mater. Char. 151 (2019) 563–581 https://doi.org/10.1016/j.matchar.2019.03.047.
[77] H. Sato, Y. Watanabe, Three-dimensional microstructural analysis of fragmentation behavior of platelet Al3Ti particles in Al-Al3Ti composite deformed by equal-channel angular pressing, Mater. Char. 144 (2018) 305–315 https://doi.org/10.1016/j.matchar.2018.07.005.
[78] Y. Han, J. Li, G. Huang, Y. Lv, X. Shao, W. Lu, D. Zhang, Effect of ECAP numbers on microstructure and properties of titanium matrix composite, Mater. Des. 75 (2015) 113–119 https://doi.org/10.1016/j.matdes.2015.03.018.
[79] R. Shobha, C. Siddaraju, K.R. Suresh, H.B. Niranjan, Mechanical property evaluation of heat treated insitu Al- TiB2 composite after severe plastic deformation, Mater. Today Proc. 5 (2018) 2534–2540.
[80] R. Pippan, S. Scheriau, A. Taylor, M. Hafok, A. Hohenwarter, A. Bachmaier, Saturation of fragmentation during severe plastic deformation, Annu. Rev. Mater. Res. 40 (2010) 319–343, https://doi.org/10.1146/annurev-matsci-070909-104445.
[81] M. Kawasaki, R.B. Figueiredo, T.G. Langdon, An investigation of hardness homogeneity throughout disks processed by high-pressure torsion, Acta Mater. 59 (2011) 308–316.
[82] Z. Zhang, D.L. Chen, Consideration of Orowan strengthening effect in particulate-reinforced metal matrix nanocomposites: a model for predicting their yield strength, Scr. Mater. 54 (2006) 1321–1326.
[83] Walter D. Pilkey, Deborah F. Pilkey, Peterson's Stress Concentration Factors, third ed., A Wiley-Interscience Publications, 978-0-470-04824-5, 2008.
[84] M. Chmielewski, K. Pietrzak, M. Teodorczyk, S. Nosewicz, D. Jarzabek, R. Zybała, P. Bazarnik, M. Lewandowska, A. Strojny-Nedza, Effect of metallic coating on the properties of copper-silicon carbide composites, Appl. Surf. Sci. 421A (2017) 159–169.
[85] E.O. Hall, The deformation and ageing of mild steel III discussion of results, Proc. Phys. Soc. Sect. B 64 (1951) 747–753.
[86] N.J. Petch, The cleavage strength of polycrystals, J. Iron Steel Inst. 174 (1953) 25–28.
[87] J. Omotoyinbo, I.O. Oladele, W. Shokoya, Effect of the degree of plastic deformation on the electrical resistance and thermal conductivity of Al-Mg-Si alloy, Leonardo Electron. J. Pract. Technol. 13 (2014) 37–50.
[88] O.V. Gendelman, M. Shapiro, Y. Estrin, R.J. Hellmig, S. Lekhtmakher, Grain size distribution and heat conductivity of copper processed by equal channel angular pressing, Mater. Sci. Eng. A 434 (2006) 88–94 https://doi.org/10.1016/j.msea.2006.06.091.
[89] P.J. Bolt, N.A.P.M. Lamboo, P.J.C.M. Rozier, Feasibility of warm drawing of Aluminium products, J. Mater. Process. Technol. 115 (1) (2001) 118–121.
[90] R. Riahifar, S. Serajzadeh, Three dimensional model for hot rolling of aluminium alloys - thermal conductivity of 6063 aluminium alloy, Mater. Des. 28 (8) (2007) 2366–2372.
[91] K. Termentzidis, M. Isaiev, A. Salnikova, I. Belabbas, D. Lacroix, J. Kioseoglou, Impact of screw and edge dislocations on the thermal conductivity of individual nanowires and bulk GaN: a molecular dynamics study, Phys. Chem. Chem. Phys. 20 (2018) 5159–5172, https://doi.org/10.1039/C7CP07821H.
[92] S.I. Kim, K.H. Lee, H.A. Mun, H.S. Kim, S.W. Hwang, J.W. Roh, D.J. Yang, W.H. Shin, X.S. Li, Y.H. Lee, G.J. Snyder, S.W. Kim, Dense dislocation arrays embedded in grain boundaries for high-performance bulk thermoelectrics, Science 348 (2015) 109–114, https://doi.org/10.1126/science.aaa4166.